3228 *Chem. Mater.* **2009,** *21,* 3228–3233
DOI:10.1021/cm9007365

CHEMISTRY OF MATERIALS
Article

Cobalt Oxide Aerogels of Ideal Supercapacitive Properties Prepared with an Epoxide Synthetic Route

Te-Yu Wei, Chun-Hung Chen, Kuo-Hsin Chang, Shih-Yuan Lu,* and Chi-Chang Hu*

Department of Chemical Engineering, National Tsing-Hua University, Hsin-Chu, Taiwan 30013, Republic of China

Received March 16, 2009. Revised Manuscript Received May 25, 2009

Mesoporous structures of high specific surface areas and high porosities, such as aerogels, are ideal for supercapacitor applications. This idea was successfully demonstrated for the first time by taking cobalt oxide aerogels as an example. Cobalt oxide aerogels of excellent supercapacitive properties, including high specific capacitances (the highest ever reported for cobalt oxides, >600 F/g at a high mass loading of 1 mg/cm^2) and onset frequencies, and excellent reversibility and cycle stability, were successfully synthesized with an epoxide addition procedure by using cobalt nitrate as the precursor. The present development makes possible the low cost production of high performance supercapacitors of the asymmetric type.

Introduction

Supercapacitors, an important energy storage device, offer transient but extremely high powers for time-dependent power needs of modern electronics and power systems. Unlike carbon materials, metal oxide based supercapacitors possess not only electric double layer capacitances but also pseudocapacitances. Transition metal oxides are particularly favored for their cost advantages over noble metal oxides such as RuO_2. Cobalt oxide, because of its favorable capacitive characteristics and environmental friendliness, received much research attention in recent years.[1−4] In general, the specific capacitance of an electrode is closely related to the specific surface area and pore size distribution of the electrode material.[1−5] Higher specific surface areas enable formation of a larger amount of double layers and accommodate more superficial electroactive species to participate in pseudocapacitive reactions. In addition, suitable pore sizes, 2−5 nm, of the porous electrode material can ease the mass transfer of electrolytes within the pores for fast redox reactions and double-layer charging/discharging.[5−10] Consequently, mesoporous structures, such as aerogels, of transition metal oxides of high specific surface areas and abundant mesopores should make a good electrode for supercapacitor applications. The preparation of aerogels of transition metal oxides, however, is not a trivial task.

Aerogels are a class of mesoporous materials possessing high specific surface areas and porosities,[11,12] from which promising applications in high temperature thermal insulation, low dielectric constant thin films, low refractive index glass, catalysts, and absorbents have been extensively investigated.[13−16] Traditionally, aerogels are prepared via sol−gel processes with alkoxides as the precursors. These alkoxides are often expensive and sensitive to moisture and heat, requiring careful handling.[17−19] In recent years, to tackle these drawbacks, epoxide synthetic routes, enabling use of low cost and stable metal salts as precursors, were successfully developed to prepare metal oxide aerogels. The success of this method, however, was restricted to aerogels prepared from precursors with the oxidation state of the metal ion not lower than 3, such as iron oxide, tin oxide, ceria, and so forth.[20−26] Gash et al. reported that some technologically important metal oxide aerogels, derived from precursors of divalent metal ions (e.g., Ni^{2+}, Co^{2+},

*To whom correspondence should be addressed. S.-Y.L.: sylu@mx.nthu.edu.tw, Fax: +886-3-571-5408, Tel: +886-3-571-4364. C.-C.H.: cchu@che.nthu.edu.tw, Fax: +886-3-571-5408, Tel: +886-3-573-6027.

(1) Lin, C.; Ritter, J. A.; Popov, B. N. *J. Eletrochem. Soc.* **1998**, 145, 4097.
(2) Srinivasan, V.; Weidner, J. W. *J. Power Sources* **2002**, 108, 15.
(3) Cao, L.; Lu, M.; Li, H. L. *J. Electrochem. Soc.* **2005**, 152, A871.
(4) Hu, C. C.; Hsu, T. Y. *Electrochim. Acta* **2008**, 53, 2386.
(5) An, K. H.; Kim, W. S.; Park, Y. S.; Choi, Y. C.; Lee, S. M.; Chung, D. C.; Bae, D. J.; Lim, S. C.; Lee, Y. H. *Adv. Mater.* **2001**, 13, 497.
(6) Zhou, H.; Li, D.; Hibino, M.; Honma, I. *Angew. Chem., Int. Ed.* **2005**, 44, 797.
(7) Huggins, R. A. *Solid State Ionics* **2000**, 134, 179.
(8) Cao, L.; Xu, F.; Liang, Y. Y.; Li, H. L. *Adv. Mater.* **2004**, 16, 1853.
(9) Hu, C. C.; Wang, C. C. *Electrochem. Commun.* **2002**, 4, 554.
(10) Chang, K. H.; Hu, C. C. *Appl. Phys. Lett.* **2006**, 88, 193102.
(11) Hüsing, N.; Schubert, U. *Angew. Chem., Int. Ed.* **1998**, 37, 22.
(12) Pierre, A. C.; Pajonk, G. M. *Chem. Rev.* **2002**, 102, 4243.
(13) Wei, T. Y.; Chang, T. F.; Lu, S. Y. *J. Am. Ceram. Soc.* **2007**, 90, 2003.
(14) Wei, T. Y.; Kuo, C. Y.; Hsu, Y. J.; Lu, S. Y.; Chang, Y. C. *Microporous Mesoporous Mater.* **2008**, 112, 580.
(15) Wei, T. Y.; Lu, S. Y.; Chang, Y. C. *J. Chin. Inst. Chem. Eng.* **2007**, 38, 477.
(16) Wei, T. Y.; Lu, S. Y.; Chang, Y. C. *J. Phys. Chem. B* **2008**, 112, 11881.
(17) Dagan, G.; Tomkiewicz, M. *J. Phys. Chem.* **1993**, 97, 12651.
(18) Baudrin, E.; Sudant, G.; Larcher, D.; Dunn, B.; Tarascon, J. M. *Chem. Mater.* **2006**, 18, 4369.
(19) Sui, R.; Rizkalla, A. S.; Charpentier, P. A. *Langmuir* **2006**, 22, 4390.
(20) Gash, A. E.; Tillotson, T. M.; Satcher, J. H., Jr.; Poco, J. F.; Hrubesh, L. W.; Simpson, R. L. *Chem. Mater.* **2001**, 13, 999.
(21) Gash, A. E.; Tillotson, T. M.; Satcher, J. H., Jr.; Hrubesh, L. W.; Simpson, R. L. *J. Non-Crystal. Solid* **2001**, 285, 22.
(22) Reibold, R. A.; Poco, J. F.; Baumann, T. F.; Simpson, R. L.; Satcher, J. H., Jr. *J. Non-Cryst. Solid* **2004**, 341, 35.
(23) Long, J. W.; Logan, M. S.; Rhodes, C. P.; Carpenter, E. E.; Stroud, R. M.; Rolison, D. R. *J. Am. Chem. Soc.* **2004**, 126, 16879.
(24) Baumann, T. F.; Kucheyev, S. O.; Gash, A. E.; Satcher, J. H., Jr. *Adv. Mater.* **2005**, 17, 1546.
(25) Kucheyev, S. O.; Baumann, T. F.; Cox, C. A.; Wang, Y. M.; Satcher, J. H., Jr.; Hamza, A. V. *Appl. Phys. Lett.* **2006**, 89, 041911.
(26) Robert, C. L.; Long, J. W.; Lucas, E. M.; Pettigrew, K. A.; Stroud, R. M.; Doescher, M. S.; Rolison, D. R. *Chem. Mater.* **2006**, 18, 50.

Published on Web 06/29/2009

Zn^{2+}, Mn^{2+}, and Cu^{2+}), could not be obtained with this technique.[21] Recently, aerogels of nickel, zinc, and copper oxides, however, have been successfully prepared with the epoxide synthetic route through careful control of the solution pH.[27−29] In this article, we report the first successful epoxide synthesis of cobalt oxide aerogels from cobalt salts. The resulting cobalt oxide aerogels were found to exhibit outstanding supercapacitive properties, possessing excellent reversibility and cycle stability and high specific capacitances and onset frequencies. The electrochemical impedance spectroscopic (EIS) spectra of these cobalt oxide aerogels approximated the characteristics of a simple RC (a resistor in series with a capacitor) circuit, implying an ideal capacitive behavior of the aerogel electrode. The specific capacitances of the aerogels prepared at a preferred processing condition exceeded 600 F/g, the highest ever reported for cobalt oxides. More importantly, these specific capacitances were determined at a high sample loading of 1 mg/cm^2, about 1 order of magnitude higher than the usual measurement practice, showing strong applicability.

Experimental Methods

Preparation of Cobalt Oxide Aerogels and Porous Cobalt Oxide Containing Micropores. The cobalt oxide aerogels were prepared with the epoxide addition procedure, followed by supercritical carbon dioxide drying. $CoCl_2 \cdot 6H_2O$ and $Co(NO_3)_2 \cdot 6H_2O$ were taken as the precursors, but only the nitrate worked to form gels. In a typical run, $Co(NO_3)_2 \cdot 6H_2O$ (0.466 g, 1.6 mmol) was first dissolved in 3.5 mL of methanol, followed by addition of propylene oxide (0.93 g, 16 mmol) to the clear solution. The solution was stirred for 10 min and then let still to gel at room temperature. The gel was obtained within 12 h. The wet gel was then washed with ethanol several times to remove the methanol and byproduct from the pores of the wet gel. The wet gel was then dried with a supercritical dryer (SAMDRI-795, Tousimis, U.S.A.). The sample was first immersed in liquid carbon dioxide for 5 h. Then, the temperature of the dryer was raised to 45 °C with the pressure maintained at 1200 psi for 2 h. After that, the system was depressurized at a slow rate to ambient pressure to obtain the dried aerogel. The dried aerogels were cobalt hydroxide in composition and needed to be further calcined at a temperature equal to or higher than 200 °C for 5 h to conver to cobalt oxide. Note that if $CoCl_2 \cdot 6H_2O$ (0.38 g 1.6 mmol) was taken as the precursor, precipitates formed within 6 min after the addition of propylene oxide. The porous cobalt oxide containing both micropores and mesopores was prepared by using MCM-41 powders as the template. An amount of 0.2 g of MCM-41 powder was dispersed in 2 mL of a 0.8 M $Co(NO_3)_2 \cdot 6H_2O$/EtOH solution, and the resulting solution was stirred at room temperature for 1 h. EtOH was removed by heating the solution to 80 °C for 24 h. After the EtOH removal, the sample was calcined at 200 °C for 5 h to obtain the porous cobalt oxide. The MCM-41 template was removed by immersion in 1 M NaOH for 1 day, followed by DI water rinsing. Finally, the rinsed sample was dried at 60 °C for 1 day.

Characterizations. The pH values of the solution were measured with a pH meter (TS-100, Suntex). The XRD patterns of the samples were recorded with an X-ray powder diffractometer (Cu Kα, Ultima IV, Rigaku). The samples were ground into fine powders for the measurements at a scan rate of 2°/min. The grain sizes of the cobalt oxides were determined with the Scherrer equation. The specific surface areas, pore volumes, and average pore sizes were obtained from the N_2 adsorption/desorption analyses conducted at 77 K (NOVA e1000, Quantachrome). The BET specific surface areas were calculated from the adsorption isotherms at the relative pressure range of 0.1−0.3, and the BJH pore volumes were determined from the desorption isotherms. The micropore volume and micropore surface area were determined with the *t*-plot method, taking nonporous silica as the reference. The pore sizes and pore size distributions were obtained through the NLDFT (non-local density functional theory) simulations. The micropore size distribution of sample PCO-micro was determined with the DA (Dubinin-Astakhov) method. The thermogravimetric analysis was run from room temperature to 500 °C at a heating rate of 5 °C/min (TGA951, Dupont instruments).

Cyclic voltammetric measurements (CHI660C, CH Instruments Inc.) were conducted in a three-electrode system in a 1 M NaOH solution. One milligram of the sample was coated on a graphite electrode as the working electrode. The reference electrode and counter electrode were Ag/AgCl and platinum, respectively. The potential was scanned between −0.1 and 0.55 V with different sweep rates. An impedance spectrum analyzer, IM6 (ZAHNER), equipped with Thales software, was employed to measure and analyze the impedance spectra. The potential amplitude of the ac was set at 10 mV, and the frequency ranged from 0.1 to 10 000 Hz.

Results and Discussion

The gel formation mechanism of the epoxide synthetic route has been intensively studied.[20−26] Briefly, epoxides act as a proton scavenger to deprotonate hydrated metal ions, which can then proceed with further hydrolysis and condensation to form gels under weak acidic conditions. The protonated epoxide undergoes ring opening, by attacks from neucleophiles such as water, nitrate ions, and chloride ions. Protons may be formed at the ring-opening step, depending on the kind of neucleophile present. To favor gel formation, slow and uniform increase of the solution pH to weak acidic conditions is necessary.[20−26] In this work, two different cobalt salts, nitrate and chloride, were tested with five different polar protic solvents including water, methanol, ethanol, isopropyl alcohol, and acetone. The two cobalt salts exhibited good solubility in water and methanol, but the strong neucleophilicity of water created unwanted protons when attacking the protonated epoxide ring, suppressing the necessary pH increase of the solution.[20] On the other hand, the ring-opening caused by the attacks of chloride ions, although producing no protons,[20] led to a too fast increase in solution pH as shown in Figure 1a by consuming the protonated epoxide and speeding up the proton scavenging of epoxide from hydrated metal ions, resulting in formation of nanoparticle precipitates. As shown in the inset of Figure 1a, when placed up side down, the precipitates of the unstable wet gel fell to the opening end of the sealed tube for the chloride case, whereas a stable gel was formed and remained on top

(27) Gash, A. E.; Satcher, J. H., Jr.; Simpson, R. L. *J. Non-Cryst. Solid* **2004**, 350, 145.
(28) Gao, Y. P.; Sisk, C. N.; Hope-Weeks, L. *J. Chem. Mater.* **2007**, 19, 6007.
(29) Sisk, C. N.; Hope-Weeks, L. J. *J. Mater. Chem.* **2008**, 18, 2607.

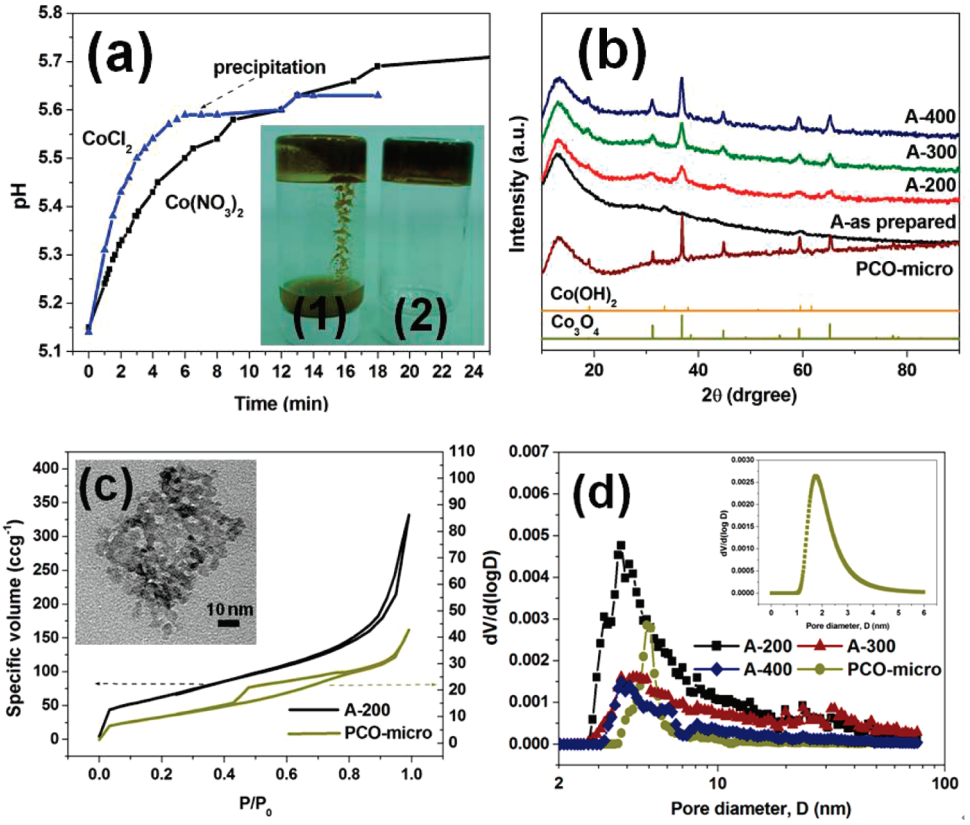

Figure 1. (a) pH evolution curves after propylene oxide addition for (1) $CoCl_2$ and (2) $Co(NO_3)_2$ cases; inset shows the falling of precipitates for the chloride case. (b) XRD patterns of the as-prepared cobalt oxide aerogel and samples A-200, A-300, A-400, and PCO-micro. The broad diffraction peak centering at the 2θ of 13° was contributed by the sample holder. (c) N_2 adsorption/desorption isotherms, conducted at 77 K, of samples A-200 and PCO-micro. The inset is a typical TEM image of sample A-200. (d) Pore size distributions of samples A-200 (solid square), A-300 (solid triangle), A-400 (solid diamond), and PCO-micro (solid circle). The inset shows the micropore distribution of sample PCO-micro.

for the nitrate case. As evident from Figure 1a, the pH increase was slower and smoother for the nitrate case than that for the chloride case, and the pH values of the reacting solution leveled off to a weak acidic condition. When the other three solvents, ethanol, isopropyl alcohol, and acetone, were used, precipitates formed because of their insufficient solubility toward the precursors.

To address the issue of pore size effect on the capacitive behavior of cobalt oxides, we prepared also porous cobalt oxides containing both micropores and mesopores for comparison purposes. One would expect a sharper decrease in specific capacitances with increasing sweep rates for electrodes containing micropores, since, upon variation of the applied potential, the severe mass transfer resistance experienced in the micropores retards the necessary electrochemical processes. The preparation of the micropore-containing porous cobalt oxides was achieved by taking the microporous MCM-41 as the template, as detailed in the Experimental Section.

The XRD patterns of the aerogels calcined at 200, 300, and 400 °C, denoted as samples A-200, A-300, and A-400, are shown in Figure 1b. Also included is the XRD pattern for the micropore-containing porous cobalt oxide calcined at 200 °C (termed PCO-micro for convenience). The as-prepared aerogel is in the crystalline form of $Co(OH)_2$ (JCPD no. 74-1057). Evidently, all samples were converted into Co_3O_4 (JCPD no. 78-1970) after the thermal treatment, and a temperature of 200 °C was high enough to drive the conversion. This can be further verified with the thermogravimetric analysis presented in Figure S1 (Supporting Information), which shows a sharp drop in sample weight at around 200 °C, indicating the occurrence of a weight losing conversion reaction. The grain size of the Co_3O_4 aerogels, as determined from the Scherrer equation, increased from 8 to 12 nm with increasing treatment temperature from 200 to 400 °C, a direct evidence of the grain growth at elevated temperatures.

Figure 1c shows the N_2 adsorption/desorption isotherms of samples A-200 and PCO-micro. All aerogel samples, although only the result for sample A-200 shown here, exhibited type IV isotherms and type H3 hysteresis loops, typical for mesoporous materials. As for sample PCO-micro, the types of isotherm and loop cannot be unambiguously identified since the sample contains both micropores and mesopores. In Table 1, we tabulate the BET specific surface areas and BJH pore volumes for the as-prepared, A-200, A-300, A-400, and PCO-micro samples. Sample PCO-micro was the only one identified with the existence of micropores, and half of its specific surface area was contributed by the micropores. For the N_2 adsorption/desorption isotherm of sample PCO-micro, the existence of the hysteresis loop indicates clearly the presence of mesopores. The isotherms of sample

Table 1. BET Specific Surface Areas, BJH Pore Volumes, and Specific Capacitances of Cobalt Oxide Aerogels and Porous Cobalt Oxides Containing Micropores

	BET specific surface area, m^2/g	specific surface area from micropores, m^2/g	BJH pore volume, cm^3/g	micropore volume, cm^3/g	specific capacitance, F/g
as prepared	103	0	0.361	0	
A-200	235	0	0.463	0	623
A-300	123	0	0.488	0	239
A-400	69	0	0.116	0	174
PCO-micro	38	19	0.063	0.021	41

PCO-micro showed the mixed characteristics of micropores and mesorpores.

The BET specific surface areas of the cobalt oxide aerogels increased from 103 to 235 m^2/g after the calcination at 200 °C, attributable to the pore opening resulting from the removal of the physisorbed water and solvent.[1] When the calcination temperature was increased, the BET specific surface areas, however, decreased, because of the densification of the aerogel structure and grain growth. The average pore size of the aerogels, determined from the NLDFT simulation,[30−33] nevertheless remained almost constant at around 3.8 nm, falling within the optimal pore size range of 2−5 nm for supercapacitor applications.[5−10] The pore size distributions of the three aerogel samples are shown in Figure 1d, exhibiting similar single-modal distributions centering around 3.8 nm. A typical TEM image of the aerogel sample was displayed as the inset of Figure 1c. The image was taken from sample A-200 and reveals the mesoporous nature of the aerogel. The aerogel is seen to be constructed from the connected nanoparticles of around 5 nm in size, and the pores formed are with a size of around 3−4 nm, in good agreement with the average NLDFT pore size.

The pore size distributions of sample PCO-micro are also displayed in Figure 1d. Because of the coexistence of micropores and mesopores, we plotted the pore size distributions in two separate graphs, one for the mesopores and the other for the micropores. Both pore size distributions are single modal with the mesopores centering around 4.8 nm and micropores centering around 1.7 nm.

To evaluate the potential of the present products for supercapacitor applications, the specific capacitances of the samples were determined from corresponding cyclic voltammograms (CV). The cyclic voltammograms were conducted in a three-electrode system. The samples were coated on a graphite substrate as the working electrode. The reference electrode and counter electrode were Ag/AgCl and platinum, respectively. The CV curves of samples A-200, A-300, A-400, and PCO-micro are shown in Figure 2a. The potential range spanned from −0.1 to 0.55 V, and the sweep rate was set at 25 mV/s. All CV curves show an anodic peak at around 0.47 V and a cathodic peak at about 0.4 V. These two peaks indicate the redox couple of Co_3O_4/CoOOH. All CV curves appeared quite symmetric, indicating high reversibility of the redox reaction on all oxide surfaces. The corresponding specific capacitances of the samples, based on a potential window of 0.23-0.53 V, were calculated from the CV curves and are tabulated in Table 1. Evidently, for the aerogel samples, the specific capacitance decreased with increasing the calcination temperature, consistent with the trend of the BET specific surface area. If one examines the two sets of data carefully, the correlation is quite strong, indicating the dominant influence of the specific surface area on specific capacitances.

The specific capacitance of 623 F/g of sample A-200 is much higher than those achieved by other mesoporous cobalt oxides, such as the loose-packed cobalt oxide nanocrystals[3] and the cobalt oxide xerogels.[1] More importantly, the sample loading of 1 mg/cm^2 used in the present work is much higher than the common practice of the field, often around 0.1 mg/cm^2. Higher sample loadings increase the sample thickness when coated on the substrate, thus increasing the difficulty for the diffusing electrolytes to access the internal pore surfaces of the porous electrode and increasing the pathway distances that the electrons need to travel. Consequently, higher sample loadings often lead to lower specific capacitances. The present product nevertheless still achieved high specific capacitances at high loading conditions, indicating its strong applicability. Also note that the present specific capacitances were reported at a relatively high sweep rate of 25 mV/s, much higher than the common sweep rate of 5 mV/s. Furthermore, the voltammograms recorded from our samples are much more symmetric than those from refs 1 and 3, indicating much better reversibility, one of the critical characteristics for supercapacitors. As to the specific capacitance of sample PCO-micro, the value was much lower than those of the aerogel samples, mainly because of the low specific surface area. The existence of micropores in sample PCO-micro, contributing half of the specific surface area, is also part of the reason for the low specific capacitance.

The disadvantageous effect of the presence of micropores, as compared to that of mesopores, on the capacitive performance of an electrode can be more clearly demonstrated by investigating the decay in specific capacitance resulting from increasing the sweep rate. The higher the sweep rate gets, the more severe the high mass transfer resistance of micropores retarding the necessary electrochemical processes for capacitive performances.[34−38] Figure 2b shows the curves of the

(30) Jagiello, J.; Thommes, M. *Carbon* **2004**, 42, 1225.
(31) Jagiello, J.; Thommes, M. *Carbon* **2004**, 42, 1227.
(32) Thommes, M.; Kohn, R.; Froba, M. *Appl. Surf. Sci.* **2002**, 196, 239.
(33) Thommes, M.; Smarsly, B.; Groenewolt, M.; Ravikovitch, P. I.; Neimark, A. V. *Langmuir* **2006**, 22, 756.
(34) Futaba, D. N.; Hata, K.; Yamada, T.; Hiraoka, T.; Hayamizu, Y.; Kakudate, Y.; Tanaike, O.; Hatori, H.; Yumura, M.; Iijima, S. *Nat. Mater.* **2006**, 5, 987.
(35) Ania, C. O.; Khomenko, V.; Raymundo-Pinero, E.; Parra, J. B.; Beguin, F. *Adv. Funct. Mater.* **2007**, 17, 1828.
(36) Endo, M.; Maeda, T.; Takeda, T.; Kim, Y. J.; Koshiba, K.; Hara, H.; Dresselhaus, M. S. *J. Electrochem. Soc.* **2001**, 148, A910.
(37) Xu, B.; Wu, F.; Chen, R.; Cao, G.; Chen, S.; Zhou, Z.; Yang, Y. *Electrochem. Commun.* **2008**, 10, 795.
(38) Selvan, R. K.; Perelshtein, I.; Perkas, N.; Gedanken, A. *J. Phys. Chem. C* **2008**, 112, 1825.

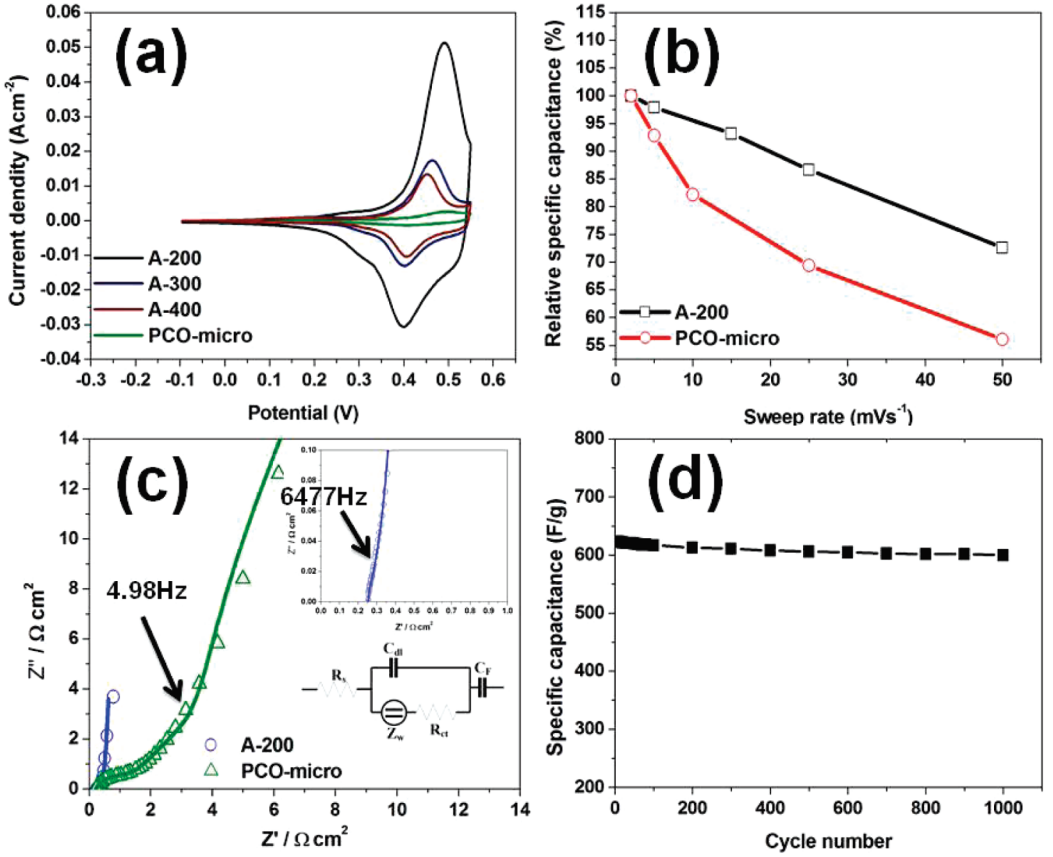

Figure 2. (a) Cyclic voltammograms of samples A-200, A-300, A-400, and PCO-micro conducted at a sweep rate of 25 mV/s. (b) Decay in specific capacitances with increasing sweep rate of the cyclic voltammorgram for samples A-200 and PCO-micro. (c) EIS spectra of samples A-200 and PCO-micro. The upper right inset shows the local enlargement at the high frequency region for sample A-200. The lower right inset is the proposed equivalent circuit to fit the EIS spectra. (d) Cycle stability test for sample A-200.

relative specific capacitances, taking the specific capacitances obtained at a sweep rate of 2 mV/s as the references, for samples A-200 and PCO-micro, versus sweep rate. Evidently, the presence of micropores in PCO-micro led to intensified decay in specific capacitances. There is also observed appreciable decay in the specific capacitance of sample A-200, although to a much less extent as compared to that of sample PCO-micro. This may be caused by the poor electronic conductivity of the cobalt oxide aerogel, particularly for the necessity of electron hopping between neighboring nanoparticles.

The more detailed characteristics of the capacitive electrode can be investigated with the electrochemical impedance spectroscopy (EIS). The EIS spectra of samples A-200 and PCO-micro conducted at 0.47 V are shown in Figure 2c. An equivalent circuit, shown as an inset of Figure 2c, was proposed to fit the spectra. The equivalent circuit is composed of a solution resistor R_s, a double layer capacitor C_{dl}, a finite-length Warburg diffusion element Z_w, a cobalt oxide-electrolyte interfacial charge transfer resistor R_{ct}, and a faradic pseudocapacitor C_F. The complicated electrochemical processes and mass transfer occurring within the pores and at the cobalt oxide−electrolyte interface were characterized as a composite interfacial impedance consisting of C_{dl} in parallel with a serial combination of Z_w and R_{ct}. The equivalent circuit was then completed by putting this composite interfacial impedance in series with R_s and C_F. Evidently, if the effect of this composite interfacial impedance is minor, then the whole equivalent circuit reduces to a simple R_sC_F circuit, indicating an ideal capacitive situation. For a simple R_sC_F circuit, the EIS spectrum is simply a vertical line intercepting the real axis at R_s. If the composite interfacial element is non-negligible, a semicircle will develop starting from the real axis intercept at R_s with decreasing frequency. From Figure 2c, it is clear that the EIS spectrum of sample A-200 mimics that of a simple R_sC_F circuit with a negligible showing of the semicircle, implying an ideal capacitive behavior of the aerogel electrode.[39] On the contrary, the EIS spectrum of sample PCO-micro shows a clear development of the semicircle, indicating the appreciable contribution of the composite interfacial element.

The onset frequency, also an important parameter for electrode materials of supercapacitors, of samples A-200 and PCO-micro can be readily determined from the EIS spectra. In this work, the onset frequency is defined as the frequency at which the lowest imaginary impedance is found or the frequency at which the impedance of the circuit starts to be dominated by its

(39) Wang, Q.; Wen, Z.; Li, J. *Adv. Funct. Mater.* **2006**, 16, 2141.

imaginary (pseudocapacitor) part in the medium frequency region.[40−42] The onset frequencies of samples A-200 and PCO-micro thus obtained were 6477 Hz and 4.98 Hz, respectively. Electrode materials with high onset frequencies are desired to deliver high powers for supercapacitors. The excellent potential of high power output of the present cobalt oxide aerogel is thus evident from its high onset frequency. Finally, the cycle stability, an important issue for capacitors for long-term applications, of sample A-200 was tested, and the results are shown in Figure 2d. The excellent cycle stability of the sample is clearly demonstrated with a negligible decay of 4% after a test of 1000 cycles.

Conclusions

In conclusion, cobalt oxide aerogels of excellent supercapacitive properties, including high specific capacitances and onset frequencies and excellent reversibility and cycle stability, were successfully synthesized with the epoxide addition procedure for the first time by using cobalt nitrate as the precursor. Cobalt oxide is a promising low cost transition metal oxide for supercapacitors of the asymmetric type, and the epoxide synthetic route enables preparation of transition metal oxide aerogels from low cost and stable metal salts instead of the much more expensive, moisture and heat sensitive alkoxides. The high specific surface area and porosity as well as the mesoporous structure of the cobalt oxide aerogel are essential for the obtained outstanding supercapacitive properties. The present development makes possible the low cost production of high performance supercapacitors of the asymmetric type.

Acknowledgment. This work was financially supported by the National Science Council of the Republic of China (Taiwan) under Grants NSC 96-2221-E-007-088-MY2 (S.-Y.L.) and NSC 97-2221-E-007-078-MY3 (C.-C.H.), and by the Top (SYL) and Boost (C.-C.H.) programs of the National Tsing-Hua University.

Supporting Information Available: TG analysis (PDF). This material is available free of charge via the Internet at http://pubs.acs.org.

(40) Hu, C. C.; Wang, C. C. *J. Electrochem. Soc.* **2003**, 150, A1079.
(41) Hu, C. C.; Wang, C. C.; Chang, K. H. *Electrochim. Acta* **2007**, 52, 2691.
(42) Huang, C. W.; Wu, Y. T.; Hu, C. C.; Li, Y. Y. *J. Power Sources* **2007**, 172, 460.